

Fermi National Accelerator Laboratory

FERMILAB-Pub-76/97-EXP
7500.456

(Submitted to Nucl. Instrum.
Methods)

STUDY OF DRIFT CHAMBER SYSTEM FOR A K-e SCATTERING EXPERIMENT AT THE FERMI NATIONAL ACCELERATOR LABORATORY

Nina A. Filatova, Turgun S. Nigmanov, Victor P. Pugachevich,
Victor D. Riabtsov, Mikhail D. Shafranov, Edouard N. Tsyganov,
Dimitry V. Uralsky, and Aleksandr S. Vodopianov
Joint Institute for Nuclear Research, Dubna, USSR

and

Fabio Sauli
CERN, Geneva, Switzerland

and

Muzaffer Atac
Fermi National Accelerator Laboratory, Batavia, Illinois 60510 USA

December 1976

STUDY OF DRIFT CHAMBER SYSTEM FOR A K-e SCATTERING
EXPERIMENT AT THE FERMI NATIONAL ACCELERATOR LABORATORY

Nina A. Filatova, Turgun S. Nigmanov, Victor P. Pugachevich,
Victor D. Riabtsov, Mikhail D. Shafranov, Edouard N. Tsyganov,
Dimitry V. Uralsky, Aleksandr S. Vodopianov

Joint Institute for Nuclear Research, DUBNA, USSR

Fabio Sauli

CERN, Geneva, Switzerland

Muzaffer Atac

Fermi National Accelerator Laboratory, Batavia, Illinois

We describe a drift chamber system for a K-e elastic scattering experiment to be done at Fermilab using a 250 GeV/c kaon beam. The chambers were built at JINR, Dubna, and tested at Fermilab using a 150 GeV/c pion beam. An average spatial accuracy of about 60 μm at low beam intensity was obtained. Drift chamber efficiencies at different beam intensities are presented. The average efficiency was more than 0.98 at intensity of 0.5×10^6 particles per spill with a FWHM beam size of about 20 mm. The dependence of drift chamber accuracy on anode high voltage and beam intensity was also studied.

1. Introduction

The kaon form factor can be accurately determined in a K-e elastic scattering experiment utilizing a 250 GeV/c K^- -beam at Fermilab. Such a high beam energy requires the use of high resolution detectors. It has been demonstrated by various experimenters¹⁻⁴ that resolutions better than 100 μm can be obtained from drift chambers. This paper shows that an average resolution of 60 μm can be obtained from the drift chambers which will be discussed below.

Chambers of two sizes, 12.5 x 12.5 cm^2 and 25 x 25 cm^2 , were constructed and tested.⁵⁻⁷ Individual planes are combined in modules, each module containing 4X and 4Y planes in one gas enclosure. Anode wires in subsequent planes are staggered to resolve the right-left ambiguity. A 25 x 25 cm^2 module is shown in Fig. 1. The modules can be easily disassembled, allowing for easy replacement of signal wires. A schematic diagram of the construction of an individual plane is shown in Fig. 2

The electric field in the drift region is shaped by wire electrodes¹⁻³ providing a sufficiently constant field of about 1500 volts/cm throughout the drift region. The chamber high voltage schematic diagram is shown in Fig. 3; a resistor divider determines negative potentials on field-shaping wires. There is a positive high voltage on signal wires, the current being limited by a 1 M Ω resistor.

Individual components are made by an epoxy-compound casting method; this method produces nearly identical planes, and also avoids many labor-consuming operations which would be necessary when building chambers from machined Fiberglass. Furthermore, the mechanical rigidity of the chamber is better. An epoxy-compound with a quartz sand filling was used to mould components of the drift chambers; all frames contain 4 mm glass strips, and the mechanical accuracy in making the frames is better than 15 microns.

The spacing of signal wires is 42 mm, so that the maximum drift length is 21 mm. The signal wires of adjacent planes are shifted by 21 mm to resolve the left-right ambiguity. Gold plated tungsten wires of 20 μ m diameter are used at a tension of 50 grams; their position accuracy is about 10 μ m.

Potential wires having 60 μ m diameter separate two neighboring drift cells. Field shaping electrodes are made from a beryllium-bronze wire of 100 μ m diameter and used at a tension of 90 grams. The space between these wires is equal to 2 mm and the position accuracy is about 15 μ m. The connection between the high voltage divider and cathode wires is made by printed circuit boards. The distance between field shaping elec-

trodes and signal wires is 3 mm to an accuracy of 15 μ m. In order to keep this distance the same when disassembling the chambers, a spacer (see Fig. 2) of calibrated thickness is used. Also, the spacer provides a smooth change of electrical field at the ends of the wires, and secures a reliable insulation in this range.

Between adjacent planes there are shielding nets of 100 μ m wire with 2 mm spacing; the distance between field shaping electrodes and shielding electrodes is 10 mm.

Individual planes are combined in modules by bushings and studs passing through centering openings at special metal inserts at the corners of frames. These openings are precision positioned so that they match from plane to plane with an accuracy of 2 μ m. A gas-tight seal is provided between frames by neoprene foam gaskets, and the gas volume is enclosed by metal frames with 60 μ m mylar-aclar windows. These frames also contain the gas inlet and outlet. The total material in an eight plane module is 0.141 g/cm (0.008 radiation lengths) in the sensitive area.

A mixture of argon (67.2%), isobutane (30.3%), and methylal (2.5%) was used as the gas. The drift velocity for this gas mixture saturates at electric fields higher than 800 V/cm,¹⁻³ the minimum electric

field in the chambers is 1500 V/cm, so that there is good time-to-space linearity. The gas mixture was commercially prepared, making the gas system convenient to operate. The accuracy of the gas mixture was certified for each bottle and typically ran to $\pm 0.5\%$ isobutane and $\pm 0.1\%$ methylal. The gas mixture was at 6 atm. pressure, and all components were gaseous at room temperature. The gas flowed at a rate of about 100 cm³/min, and typical gas leaks for one module were less than 5 cm³/min.

We used standard stabilized high voltage supplies, and did not use any other devices to limit current on the signal wire. The signals from the wire was taken through a 470 pF dividing capacitor and the 200 Ω resistor, and were detected by an amplifier-discriminator, which is attached to the chamber (see Fig. 1). The thresholds of the amplifiers could be set in the range from 4 to 15 μ A, and the output signal parameters are NIM standard.

2. Test of the Drift Chambers with Radioactive Sources

The following parameters were measured on each chamber in the laboratory tests using radioactive sources:

- a. Pulse height distribution for each wire, using a 5.9 KeV photon (Fe^{55}) source, for several values of the anode potential.
- b. Average pulse height on Fe^{55} as a function of the distance of the collimated source from the signal wire, along the drift region.
- c. Efficiency of each plane on minimum ionizing electrons, as a function of the anodic voltage.

- d. Noise or single counting rate of each plane as a function of the anodic voltage.
- e. Furthermore, time spectra of a non-collimated electron beam were recorded to check the value of the drift velocity, and a rough measurement of coordinate accuracy was obtained.

Figure 4 shows the pulse obtained on Fe^{55} using 25 Ω input impedance. The 6 mV average pulse height corresponds to about a 240 μ A peak current. Figure 5 shows that the effective pulse width, which is of primary importance for multi-track resolution, can be reduced to about 20 nsec at the 5% threshold point with a small differentiation. Figure 6 shows the pulse height spectrum at 1 k Ω input impedance: the 5.9 KeV as well as 3 KeV argon escape lines are clearly identified. Essentially, the pulse height does not depend on the distance from the wire. All wires have a similar behavior, with a wire-to-wire variation of less than 15-20%. Figure 7 shows the pulse height versus anode voltage. In the linear range, an 80 volt increase doubles the pulse height, in agreement with the results of Ref. 9. A typical plateau obtained using minimum ionizing electrons from a collimated electron source (Ru^{106}) is shown in Fig. 8. The particles were detected by a telescope composed of two scintillation counters. A good operating voltage is -3.5 kV for the drift potential and +1.6 kV

for the anode potential. The spread of the plateau for different planes is small (20-30 V), and due mainly to the electronic threshold variation. The typical noise, or single counting rate without radioactive source, was less than 10 counts per sec per wire.

Time spectra on the wires have been recorded for a non-collimated electron source; the time spectrum is shown in Fig. 9. Estimations of the drift velocity were made from the time difference between the edges of the spectrum; the results are in good agreement with the measurements of Ref. 9. A measurement of spatial accuracy was attempted using three consecutive planes: figure 10 shows the time spectrum of the coordinate measured in one plane when the two others are used as electronic collimators. The FWHM of the distribution is 30 nsec, or ~ 1.5 mm. Of course, this is entirely due to multiple scattering in the gas of the chamber.

The tests made using radioactive sources demonstrated the agreement between the chamber parameters and their expected values. Further measurements of the drift chamber parameters were made in the M1 beam line in the Meson Laboratory at Fermilab.

3. Test of the Drift Chambers In the Beam

Two modules, one 12.5×12.5 cm² and the other 25×25 cm², were placed in a beam for the tests described in this section.⁷ The modules were separated by a distance of about one meter. Twenty signal wires in the X- and Y-planes of the first module and 28 wires in the second module in the beam area were activated.

The signal from a coincidence of two scintillation counters was used as common start for the time-to-digital converters. Drift chamber signals were delayed by cables for a time necessary to produce the start signal. To avoid electronic rate problems and the complication in detecting more than one signal from a wire, only events not preceded by a beam track within 1 μ sec, and not followed by a track within 500 nsec, were used in the analysis. These conditions assure a high spectrometer track finding efficiency, and will be used during the K-e elastic scattering experiment.

Amplifier test inputs were used for checking all the channels, for tuning amplifier thresholds, and for calibrating all time-to-digital convertings. It was possible to send a calibrated test pulse to all channels simultaneously.

The standard range of the ORTEC-EG&G TD811 time-to-digital converters was modified so that each count of the TDC corresponded to 0.25 nsec with a full range of 500 nsec. All TDC channels were calibrated by one delay box; a start signal from a generator was delayed, fanned out, and sent to all amplifier test inputs. Test triggers for different delays were written on magnetic tape, and these data were used to determine the parameters of all converters. The stability of the

time interval measurement by the TDC was practically perfect, and results were reproducible after several months. The integral non-linearity of the TDC's was less than one count over the full range.

A beam of 150 GeV/c negative particles was used to test the drift chambers in the M1 beam line of the Meson Laboratory at Fermilab. The beam size was about 20 mm (FWHM) in both X- and Y-views, and the angular divergence of the beam was less than 0.06 mrad. The spill time was about 0.9 seconds.

Data for every trigger was read out by a HP-2100 computer and was recorded on magnetic tapes for further analysis. Up to 120 triggers were taken during one spill. The data were checked in real time by an on-line software system. Plane efficiencies and accuracies for each wire were calculated, and the beam profiles for each wire were displayed.

The drift chambers were tested at different anode voltages and different beam intensities. Anode voltage was varied from 1.35 kV to 1.85 kV, and beam intensity from a few thousand to 0.5×10^6 particles per spill. Overall, about 450,000 triggers were recorded on magnetic tapes for later off-line analysis.

During the tests in the beam it was found that chambers and electronics were reliable and easy to operate. However, there were a number of problems which indicated the need for further improvements in the system. In a small percentage of triggers there were signals induced in one channel from neighboring channels ("cross-talk"). The effect is shown in Fig. 11, where distribution of events, as

a function of the number of triggered channels, is shown in the X-plane and the Y-plane in the first module. Due to the low beam intensity used during this measurement, the effect could not be attributed to accidentals; it was essentially removed by improving the grounding and shielding of the outputs. It was found also that the shielding from external sources of rf noise was insufficient. None of these effects was a serious problem in the operation of the drift chamber system or in the investigation of the chamber parameters.

4. Results of Drift Chamber Test in the Beam

Figure 12 displays the average efficiency as a function of anode voltage for the 25×25 cm² module using three different beam intensities. Curve 1 was obtained at beam intensities of about 6×10^3 particles per burst, and essentially reproduces the data obtained using the β -source. As the beam intensity increases, curves 2 and 3, the efficiency curve loses its "classical" shape because the signal amplitude spectrum changes, showing many signals of low amplitude. However, even at 0.5×10^6 particles per burst a reasonably high efficiency (98.2%) can be achieved by using high anode voltage and low electronic thresholds; this explains our improved efficiency at high beam intensity in comparison to Ref. 9.

Using a simple model of chamber operation at high intensity we can quantitatively estimate some parameters which

have an influence on the chamber efficiency. Assuming, for instance, that the size of the avalanche along the wire is about 0.2 mm, it is possible to estimate a time, T , for complete insensitivity to the detection of the next particle over the 0.2 mm range. Under our conditions T is approximately 4 μ sec.

Track selection was done using the following criteria:

- a. The times from the left and right signal wires were summed to check the drift time constancy requirement. A gaussian-like distribution was found from the summed times. Those tracks falling within ± 15 nsec deviation were accepted as good coordinate candidates.
- b. In order to avoid the need to measure wire-by-wire systematic corrections for this test, only wires on the same side of a particle trajectory were used in the following computation.

The spatial resolution of one wire was calculated by using the reconstructed trajectories of the beam particles as detected by three aligned planes, (see Fig. 13), assuming that the resolutions of all wires are equal. The root-mean-square, ϵ , of the distribution of the quantity

$$\delta = t_2 - t_1 - (t_3 - t_1) \cdot (Z_2 - Z_1) / (Z_3 - Z_1) \quad (1)$$

is related to the spatial accuracy of one wire by the expression

$$\sigma = \epsilon \cdot \omega / \sqrt{2(1 - DZ + (DZ)^2)} \quad (2)$$

in which t_1, t_2, t_3 are the drift times, Z_1, Z_2, Z_3 the z-positions of the wire planes, ω the drift velocity and $DZ =$

$(Z_2 - Z_1) / (Z_3 - Z_1)$. ϵ was obtained by fitting the δ -distribution to a gaussian form. Figure 14 shows σ vs. drift length for the 25 x 25 cm² module at low beam intensity (several thousand particles per burst), at an anode voltage +1.75 kV. The solid curve is fitted to the expression

$$A \sin(\arctg \frac{B}{X}) + C\sqrt{X} + D \quad (3)$$

where X is the drift length. The first term describes dispersion due to statistical fluctuations in the time of arrival of n th electron which produces the output signal from the amplifier, due to the finite distances between the primary ionization clusters. The second term describes the diffusion processes, and the third term describes fluctuations due to electronics, such as time slewing, etc. The first term in expression (3) is the major contributor to the error in coordinate measurement at small distances, while the second term dominates the error at large distances from the wire.

The average value of the spatial resolution shown in Fig. 14 is 60 μ m. This result is slightly better than in reference 9, and may be due to more precise readout electronics, lower amplifier thresholds, and less multiple Coulomb scattering.

The spatial resolution with respect to anode voltage was investigated. Figure 15 shows the data for the first module

of drift chambers as a group of fitted curves describing accuracy as a function of the drift length for different anode voltages. The average accuracy as a function of anode voltage is shown in Fig. 16.

The change in average accuracy with respect to anode voltage is understood to be an effect of the signal rise time. As the anode voltage is decreased (at a constant amplifier threshold), the time spread of the leading edge of the smaller signals crossing threshold increases. The closer the signal amplitude is to the threshold used, the larger the time spread due to this leading edge becomes. In addition, there is also some time slewing in the amplifier, which also increases the time spread of the output signals.

An investigation of spatial resolution vs. beam intensity was also carried out. Figure 17 shows the average accuracy of the drift chambers at different intensities using the same anode voltage of +1.75 kV. The average accuracy degrades to 85 μm at 0.5×10^6 particles per burst. It is approximately equivalent to a decrease in anode voltage of 200 V. The average accuracy is 81 μm at this intensity and at an anode voltage of +1.85 kV.

5. Track Reconstruction

The data on drift chamber accuracy, obtained by expression (1) and given in the section above, are valid in the case where all the necessary corrections and calibrations are done. Any nonlinearities or instabilities in the chamber conditions cause changes in the coordinate measurements, whereas lack of knowledge of the absolute constants, such as a drift velocity, start signal delay, etc.,

do not change the results of these calculations.

It has been shown^{2,3,9} that the drift velocity is practically independent of the electric field E at high values of E for the gas mixture of argon (67.3%), isobutane (30.2%) and methylal (2.5%). Nevertheless, even under these conditions the time-to-coordinate dependence is only approximately linear, mainly because of diffusion and ion pairs statistics close to the wire (see Fig. 14). Non-linear effects in our drift chambers are shown in Fig. 18, where the value of $t_2 + (t_1 + t_3)/2$ versus track position is displayed. Here t_1 , t_2 , t_3 are the time measurements in three consecutive planes. In the ideal case, this value should be constant; for our conditions it changes by ± 2 nanosecond.

Excluding physical nonlinear effects, slow drifts of the electronics and chamber parameters during the long time period of an experiment must be taken into account. Slow uncontrolled changes in the chamber parameters over a period of several days can change coordinates by several hundred microns.

To obtain very good spatial resolutions each channel should be treated individually; in fact, drift velocities for different channels can be slightly different. This effect is probably due to the fact that under real conditions the average amplitude of the signals is dependent on particle position (recombination and collection time effects). In this case, time-slewing of the amplifiers can cause differences

in effective drift velocities for different channels.

In a real experimental set-up with a few hundred channels in use, determining more than a thousand parameters is extremely difficult, especially since these parameters change in time. In principle, a procedure for regular and detailed calibration is necessary to solve this problem. However, this is not feasible in practice, since it leads to many complications in an experiment. At the same time, all the information necessary for calibration usually exists in the primary experimental data if one uses the fact that the tracks are straight lines. The accuracy of these parameters will depend on the number of good tracks during a time interval in which the variation of the parameters are small. In practice, the parameters can be considered as constant over several hours of data taking. Special computing methods must be developed to use the information. Of course, these methods can be dependent on the actual conditions of the experiments.

Usually, the most complicated problem is to find the minimum TDC time for each wire, t_0 . Let us consider how t_0 can be found in the structure of signal wires presented in Fig. 19. Suppose two tracks passed through the gap on two different sides of wire number 1 and through the other gaps on the same side of wires number 2 and 3. In this case, the following relation can be written:

$$S_1 - 2t_0 = d_3(1-\alpha)\omega_3/\omega_1 + d_2 \alpha\omega_2/\omega_1.$$

Here S_1 is the sum of the time intervals detected by the wire number 1 for two tracks, d_2 is the difference of time intervals for the wire number 2, d_3 is the difference of time intervals for the wire number 3, ω_1 , ω_2 , and ω_3 are the corresponding drift velocities, and

$$\alpha = (Z_3 - Z_1)/(Z_3 - Z_2),$$

where Z is the position of a wire along the beam direction. Using three pairs of tracks, one can find t_0 , ω_2/ω_1 , and ω_3/ω_1 . With high statistics these parameters can be found with very good accuracy. By this method, one can find t_0 for all the wires in the beam.

In our particular case the structure shown in the Fig. 19 could be obtained only by using two different drift chamber modules. For our geometry α was equal to about 15, and the method described above was not very precise. Instead of this, for determination of the t_0 's we used the fact that at wrong value of t_0 "cuts" appear in the angular distribution of the beam.

Below we describe some results of our program when track finding, tuning, and adjustment of the coordinate system parameters are done simultaneously.

The coordinate of the particle is calculated from the formula

$$X = X_0 \pm (t - t_0) \cdot \omega$$

where t is the measured drift time, X_0 is the position of the sense wire in the drift chamber coordinate system, t_0 is the minimum TDC time, and ω is the drift velocity. Since there is a left-right ambiguity two coordinates were calculated. The values of X_0 and t_0 were recalculated from the expressions

$$X_0 = (D_L + D_R)/2;$$

$$t_0 = \omega^{-1} \cdot (D_L - D_R)/2 + \Delta$$

where D_L and D_R are the mean deviations the left and right

coordinates from the reconstructed particle trajectory. The coordinate of the sense wire at edge of the drift chamber was calculated from the hypothesis that its t_0 is equal to the mean t_0 of the central sense wires. As was mentioned above Δ was calculated minimizing the discontinuity in the angular distribution of the particles near the sense wire resulting from using wrong value of t_0 . Small differences in the value of ω for different sense wires were calculated with constraint that the value of the deviation between measured and fitted values of the particle coordinate X were independent of the magnitude of X .

The comparison of the calculated and actual position of the wires and adjustment of the drift velocity calibrate the scale of the coordinate system.

Our program tuned the coordinate system parameters by an iterative method. Let us illustrate the results of tuning by several examples. Figure 20 shows the current value of t_0 averaged over all the wires in the first and in the second module. The current value of the averaged t_0 is presented as abscissa. Figure 20 shows that the program quickly reconstructs true values of t_0 's after any deviation of their initial values. Figure 21 shows the distribution of the mean values of track angles versus track position for one initial set of t_0 's and for the set of adjusted t_0 's. One can see that by changing the t_0 's the program makes the distribution reasonably smooth. Figure 22 shows the results concerning the corrections to drift velocities. Here the averaged value of $1/\omega$ is presented as the ordinate and the number of analyzed triggers is presented as the abscissa. One can see that the deviation of the $1/\omega$ values by $\pm 3.5\%$ from the true values does not yet destroy the convergence

of the results. Figure 23 demonstrates how the track finding efficiency changes during the run of the program in the case where the initial constants are definitely wrong. In this case the initial values of the drift velocities were made less than the true values by the 3.5%. In this version of the program, for finding a track, we require a signal to be detected in any three of the four planes in each module. The deviation of an coordinate from the fitted track should not be more than 4ξ ($\xi = 100 \mu\text{m}$).

6. Acknowledgements

We wish to express our gratitude and appreciation to all the people who provided considerable help in this work.

We are grateful to Prof. A.M. Baldin, Director of Laboratory of High Energies of JINR, without support this work would not have taken place. At JINR we have had significant support from A.A. Kuznetsov, L.G. Makarov, I.F. Kolpakov, M.F. Likhachev, I.A. Savin, V.L. Karpovsk and M.A. Liberman. Dr. I. Ioan participated in the initial stages of this work.

Professor D. Stork, UCLA, provided significant support and encouragement in this effort. The authors are grateful to Dr. T. Toohig, Fermi National Accelerator Laboratory for his support and help in all problems encountered. Professor E. Dally lent us active help in the initial preparation of the drift chambers for beam testing. We are grateful to our colleagues from Fermilab, namely: C. Brown, P. Koehler, J. Tompkins, and A. Wehmann for their help during measurements in the

beam. We wish to thank C. Kerns and L. Hardi for engineering assistance and M. Kibilko, P. Vasquez and M. Hrycyk for technical assistance on different stages of work.

The authors would like to specifically acknowledge Dr. R.R. Wilson and Dr. E.L. Goldwasser for their support and interest in this work.

References

- ¹ G. Charpak, R. Bouclier, T. Bressani, J. Favier and C. Zupancic, Nucl. Instr. & Methods 62(1968)262.
- ² G. Charpak, F. Sauli and W. Duinker, Nucl. Instr. & Methods 108(1973)413.
- ³ A. Breskin, G. Charpak, B. Gabioud, F. Sauli, N. Trautner, W. Duinker and G. Schultz, Nucl. Instr. & Methods 119(1974)9.
- ⁴ M. Atac and C. Ankenbrandt, IEEE Transactions on Nuclear Science, Vol. NS-22, February, 1975.
- ⁵ S. G. Basiladze, A.S. Vodopianov, T.S. Nigmanov, V.P. Pugachevich, D.V. Uralsky, E.N. Tsyganov and M.D. Shafranov, JINR, D12-9164, p. 28, Dubna, 1975.
- ⁶ A.S. Vodopianov, T.S. Nigmanov, V.P. Pugachevich, V.D. Riabtsov, D.V. Uralsky, E.N. Tsyganov and M.D. Shafranov, JINR, P13-9351, Dubna, 1975.
- ⁷ T.S. Nigmanov, V.P. Pugachevich, V.D. Riabtsov, M.D. Shafranov, E.N. Tsyganov, D.V. Uralsky, A.S. Vodopianov, F. Sauli, M. Atac and J. Tompkins, Fermilab-76/26-Exp, 1976.
- ⁸ S.G. Basiladze, JINR, 12-8911, Dubna, 1975.
- ⁹ A. Breskin, G. Charpak, F. Sauli, M. Atkinson and G. Shultz, Nucl. Instr. & Methods, 124(1975)189.

FIGURE CAPTIONS

- Figure 1: Drift chamber module of 25 x 25 cm² size
- Figure 2: Schematic diagram of the construction of an individual plane.
- Figure 3: Chamber high voltage schematic diagram.
- Figure 4: Pulse obtained on Fe⁵⁵ using 25Ω input impedance. Vertical scale: 2 mV/div; horizontal scale: 10 nsec/div.
- Figure 5: Pulse obtained on Fe⁵⁵ with a small differentiation. Vertical scale: 2mV/div; horizontal scale: 10 nsec/div.
- Figure 6: Pulse height spectrum at 1 kΩ input impedance on Fe⁵⁵ showing the 5.9 KeV photoelectrons and the 3 KeV argon escape.
- Figure 7: Pulse height vs. anode voltage.
- Figure 8: Efficiency plateau using minimum ionizing electrons.
- Figure 9: Time spectrum on a diffused electron source.
- Figure 10: "Accuracy" of a plane when selecting a narrow beam of electrons by using other planes.
- Figure 11: Distribution of events vs. the number of triggered channels for X- and Y-plane in the small module.
- Figure 12: Average efficiency vs. anode voltage. Curve 1 for data at an intensity of 6 x 10³ particles per burst; Curve 2, 2 x 10⁵; Curve 3, 0.5 x 10⁶.
- Figure 13: Schematic diagram of signal wires used in determining the spatial resolution of a drift chamber plane.
- Figure 14: Spatial resolution of drift chambers vs. drift length at low intensity.
- Figure 15: Curves of spatial resolution of drift chambers vs. anode voltage at low intensity.
- Figure 16: Average spatial accuracy of drift chambers vs. anode voltage.
- Figure 17: Average spatial accuracy of drift chambers vs. beam intensity.

- Figure 18: The value of $t_2 + (t_1 + t_3)/2$ for three consecutive planes. Nonlinear effects of about ± 2 nsec are seen. The solid line is an approximation in three "linear" regions. The value origin of the ordinate is relative.
- Figure 19: Positions of signal wires in the drift chamber system which are necessary to find t_0 's.
- Figure 20: Change of an average t_0 during the operation of the track-finding program. Ordinate represents t_0 , abscissa represents number of analyzed triggers.
- Top: Results for the first module.
Bottom: Results for the second module.
- Figure 21: Averaged drift velocity vs. number of analyzed triggers. Initial values deviated from the true ones by $\pm 3.5\%$.
- Figure 23: Track-finding efficiency vs. number of analyzed tracks. Initial drift velocity values are 3.5% less than true ones.

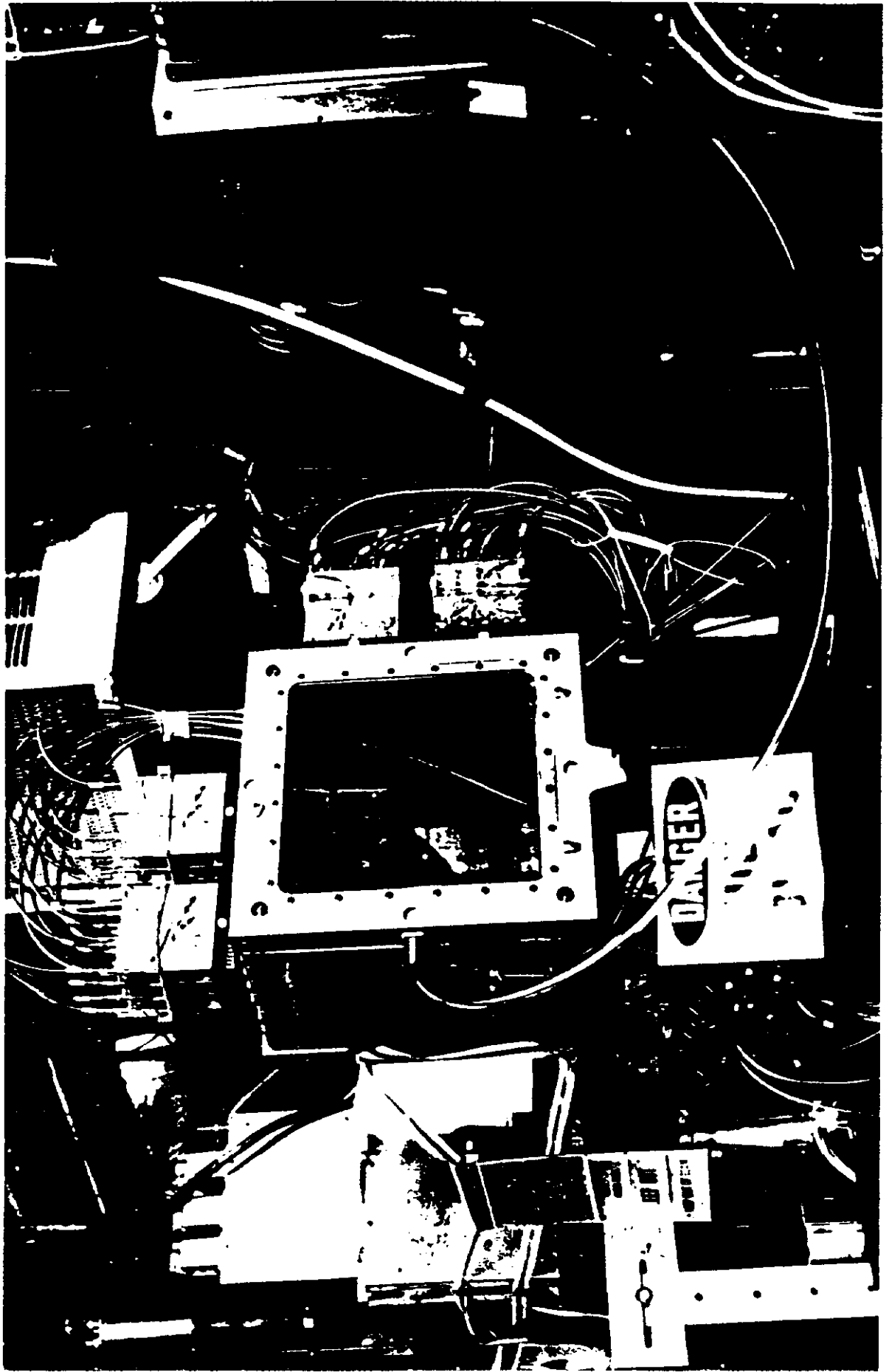


Fig. 1

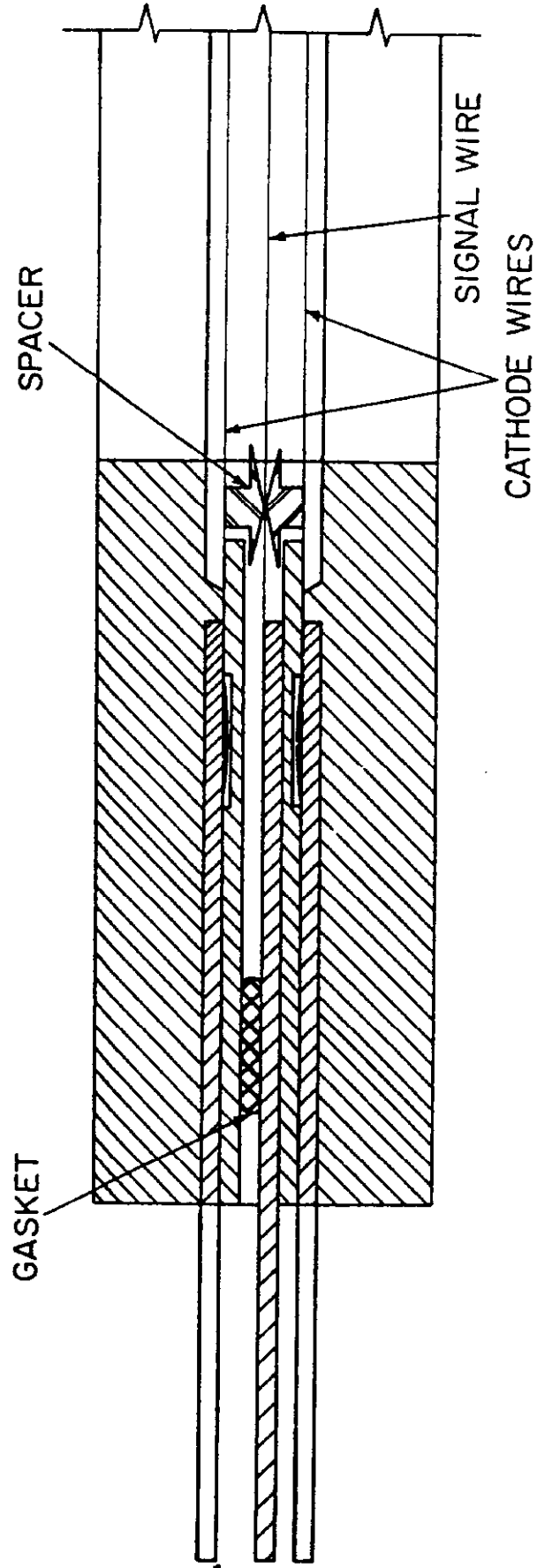


Fig. 2

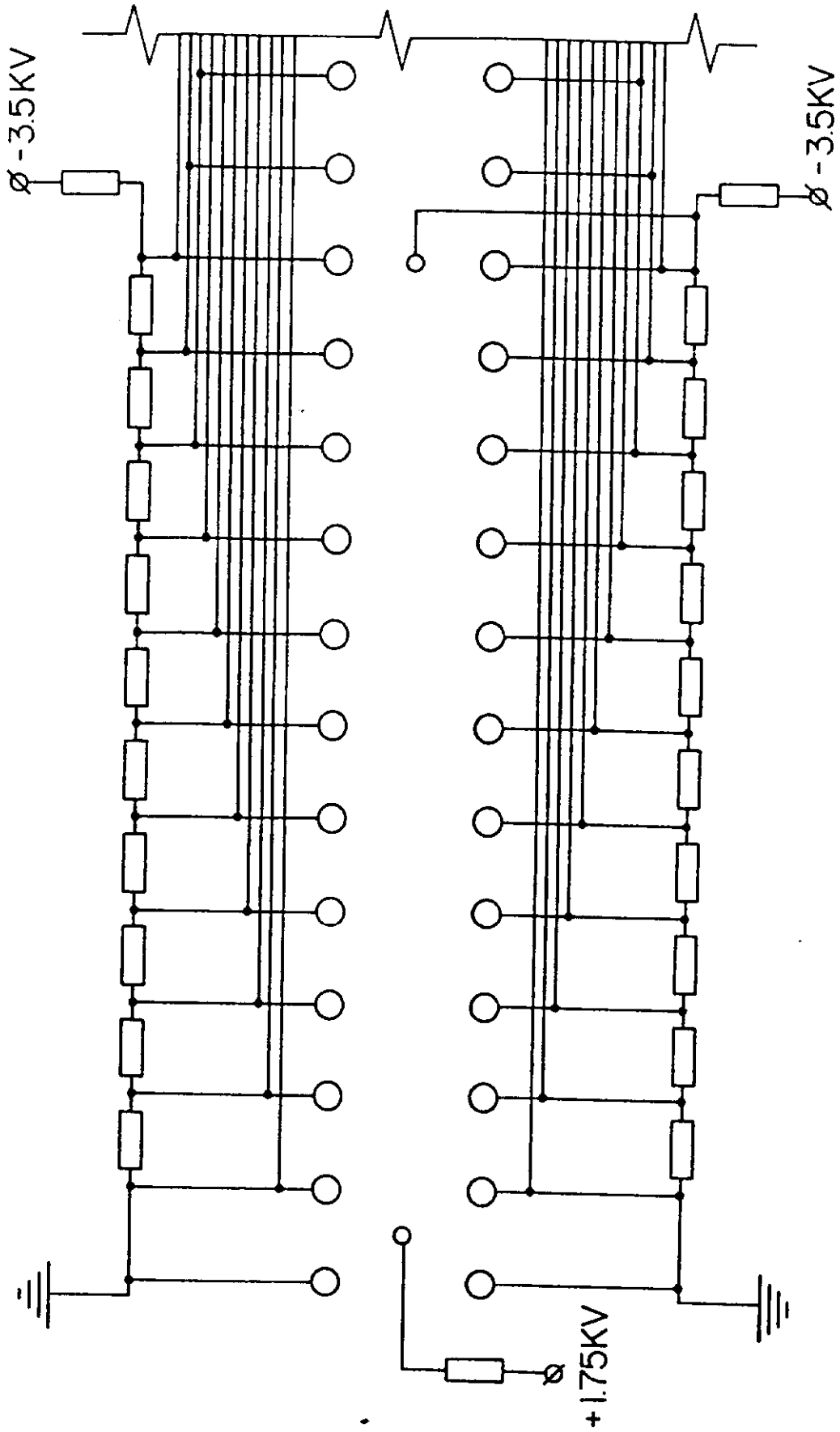
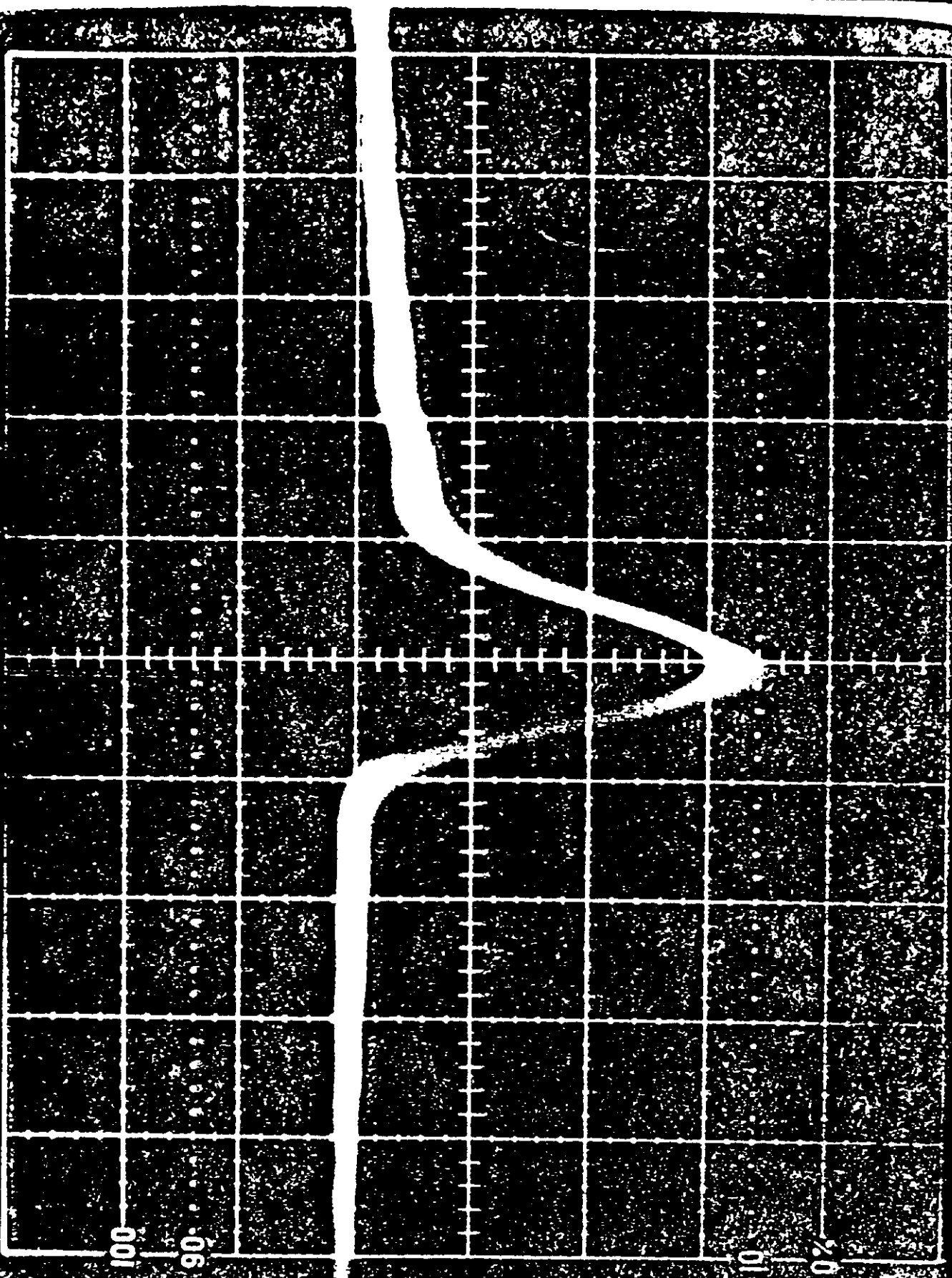
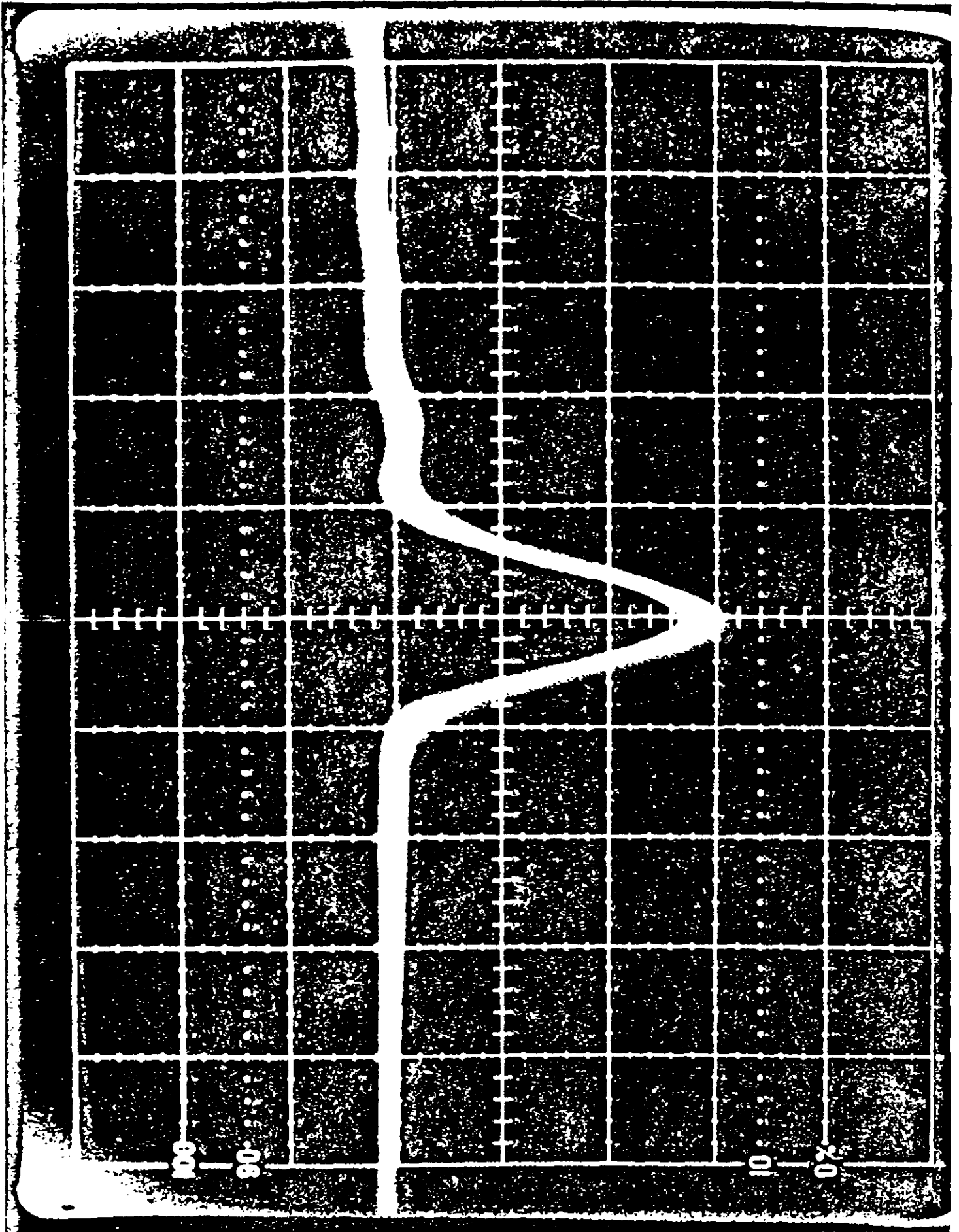


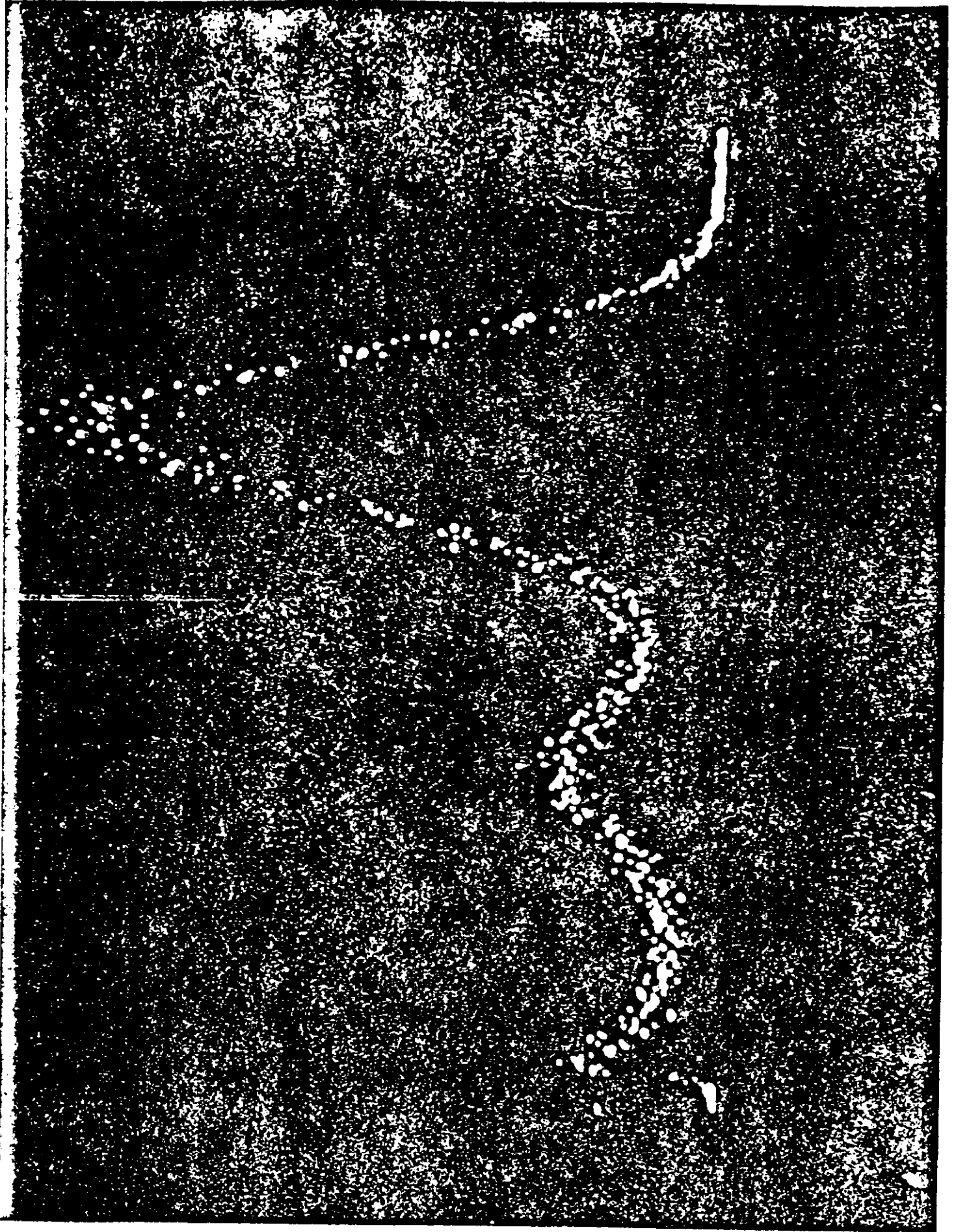
Fig. 3



100
90

10
%





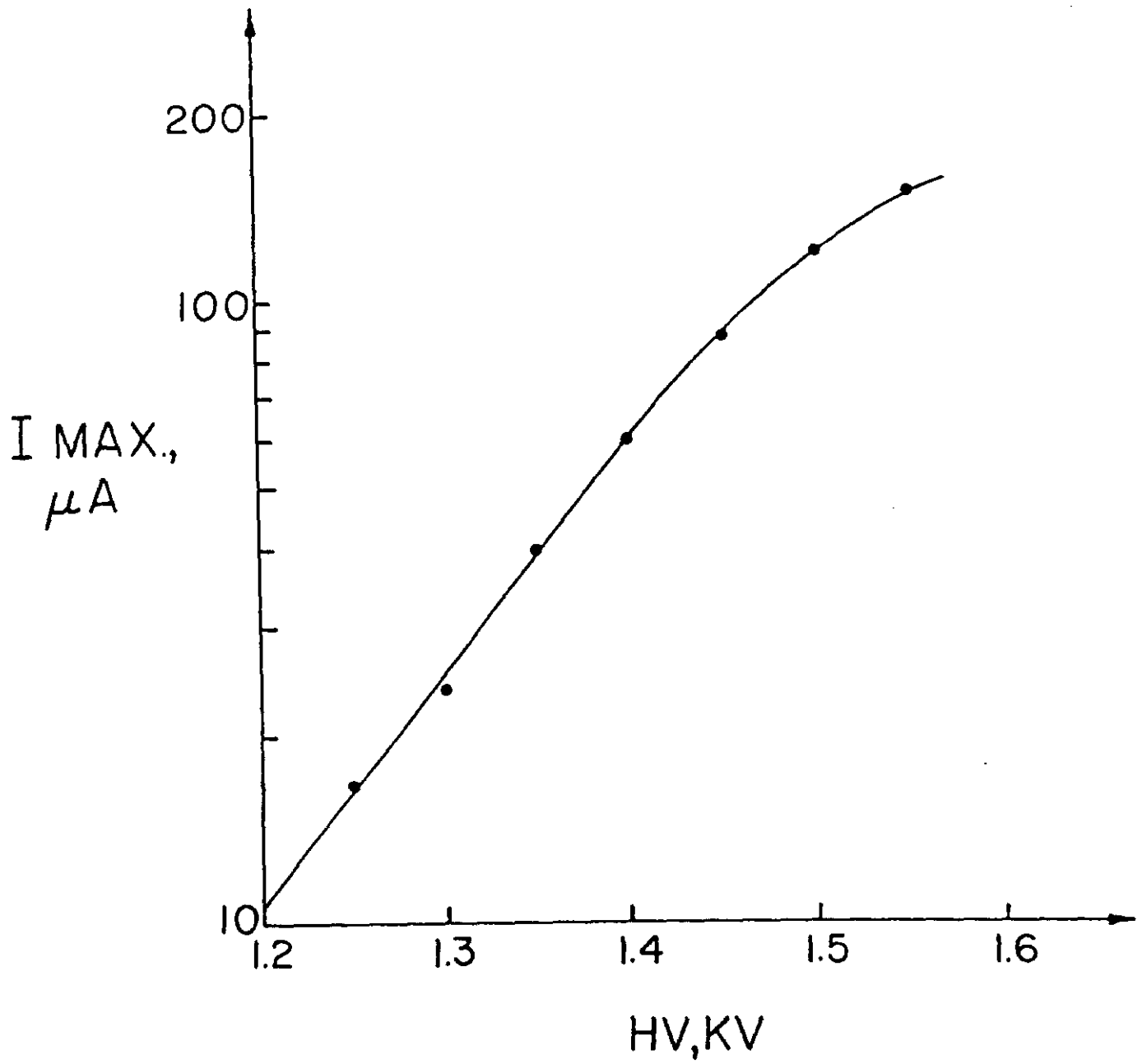


Fig. 7

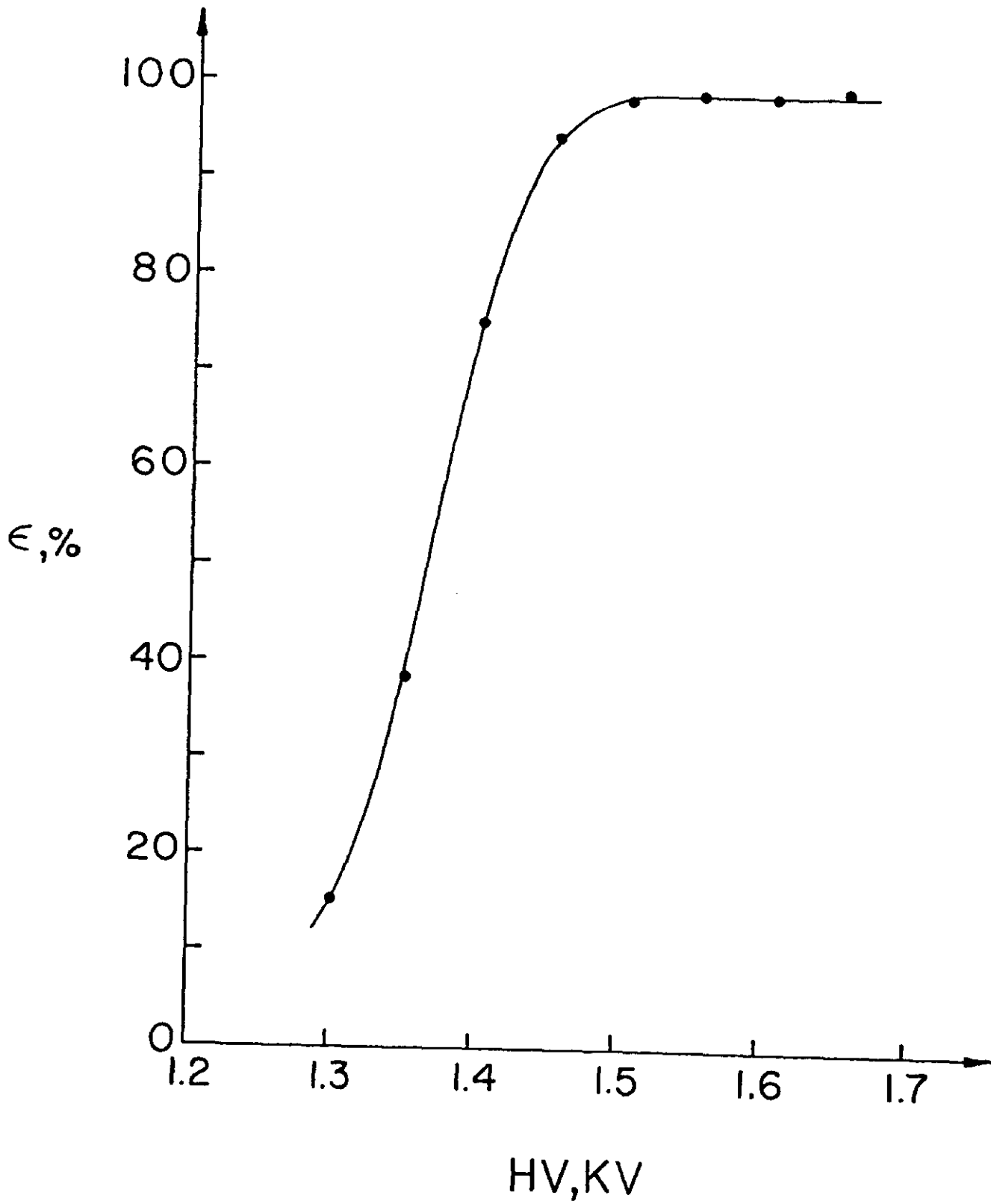


Fig. 8

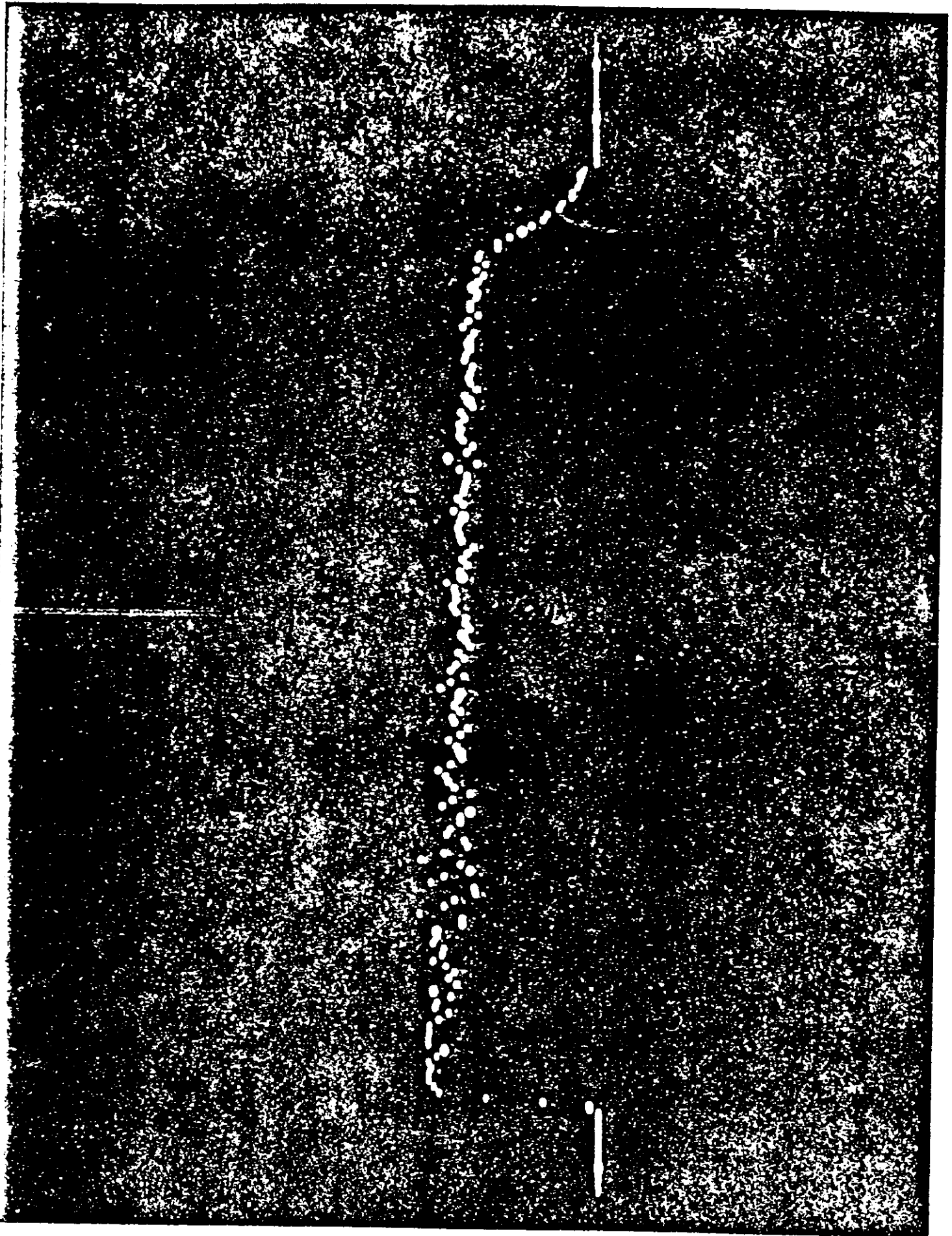


Fig. 9

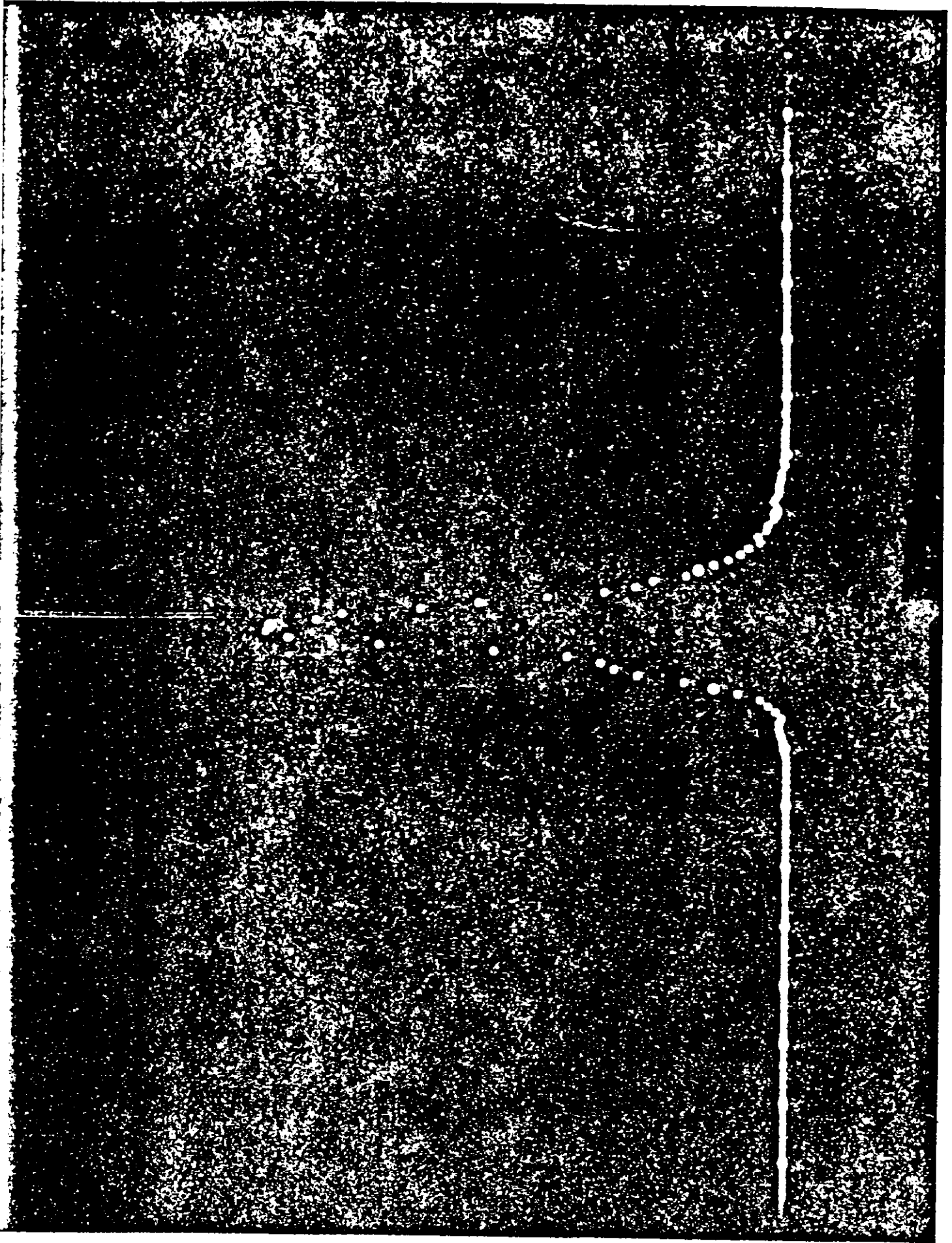


Fig. 10

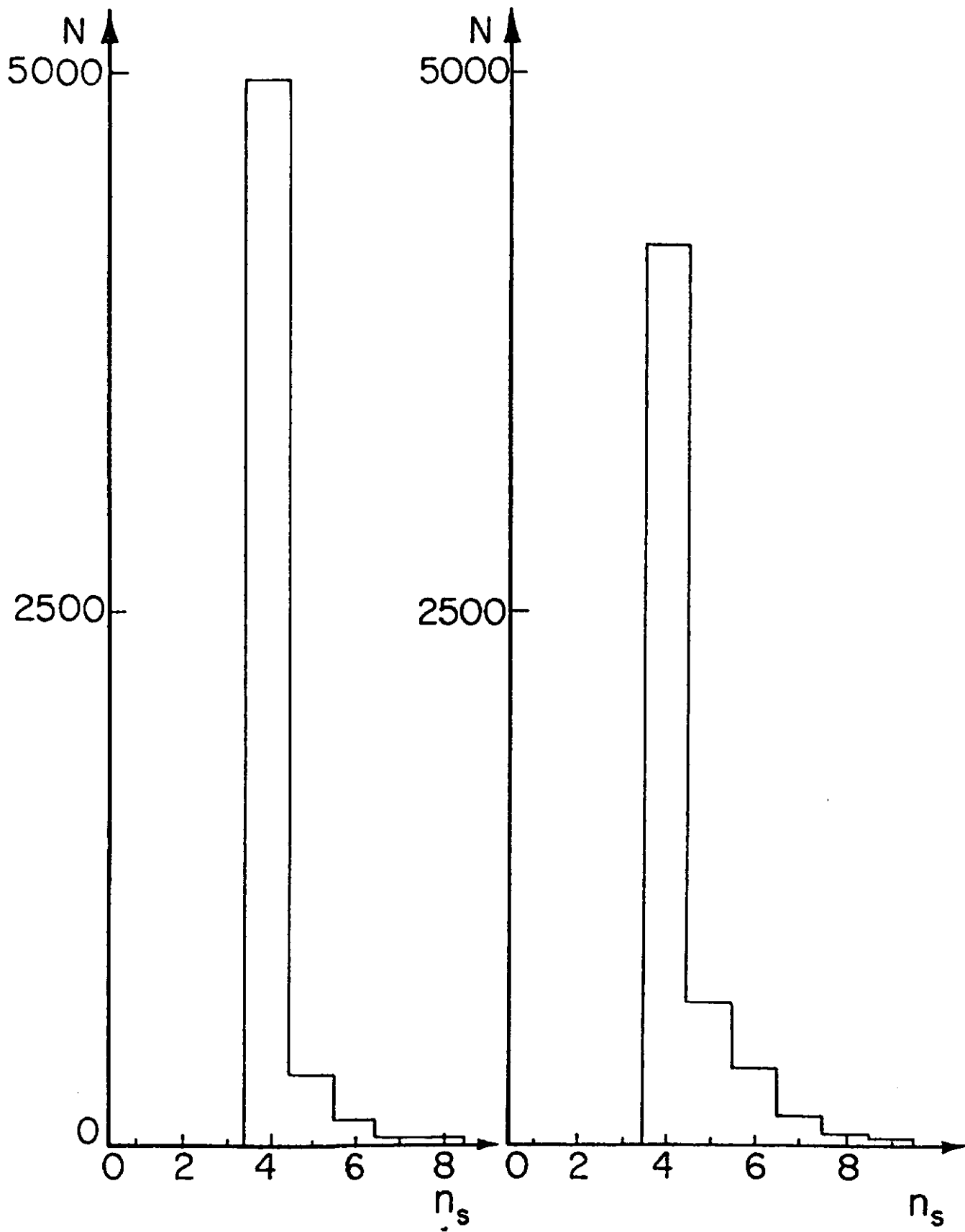


Fig. 11

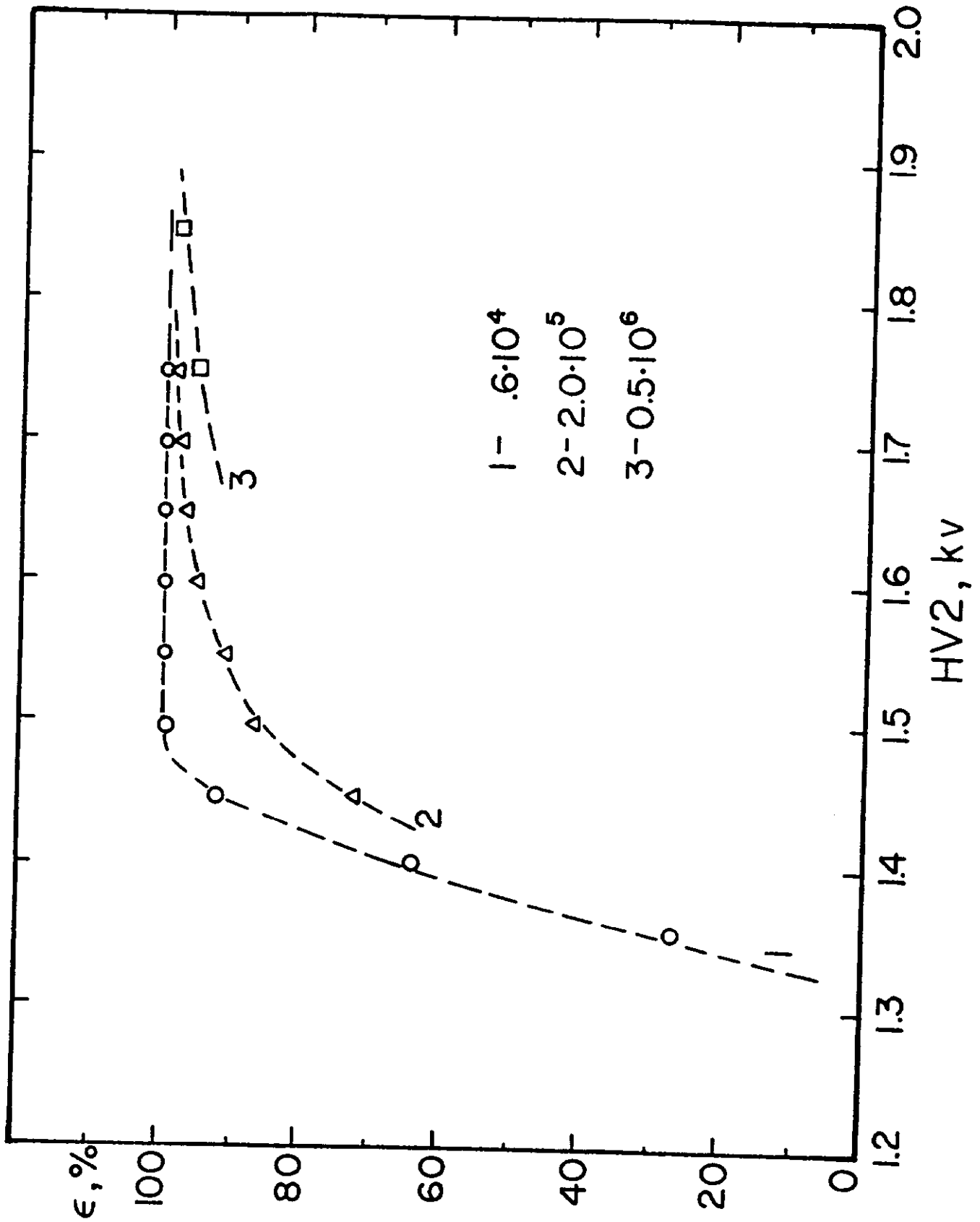


Fig. 12

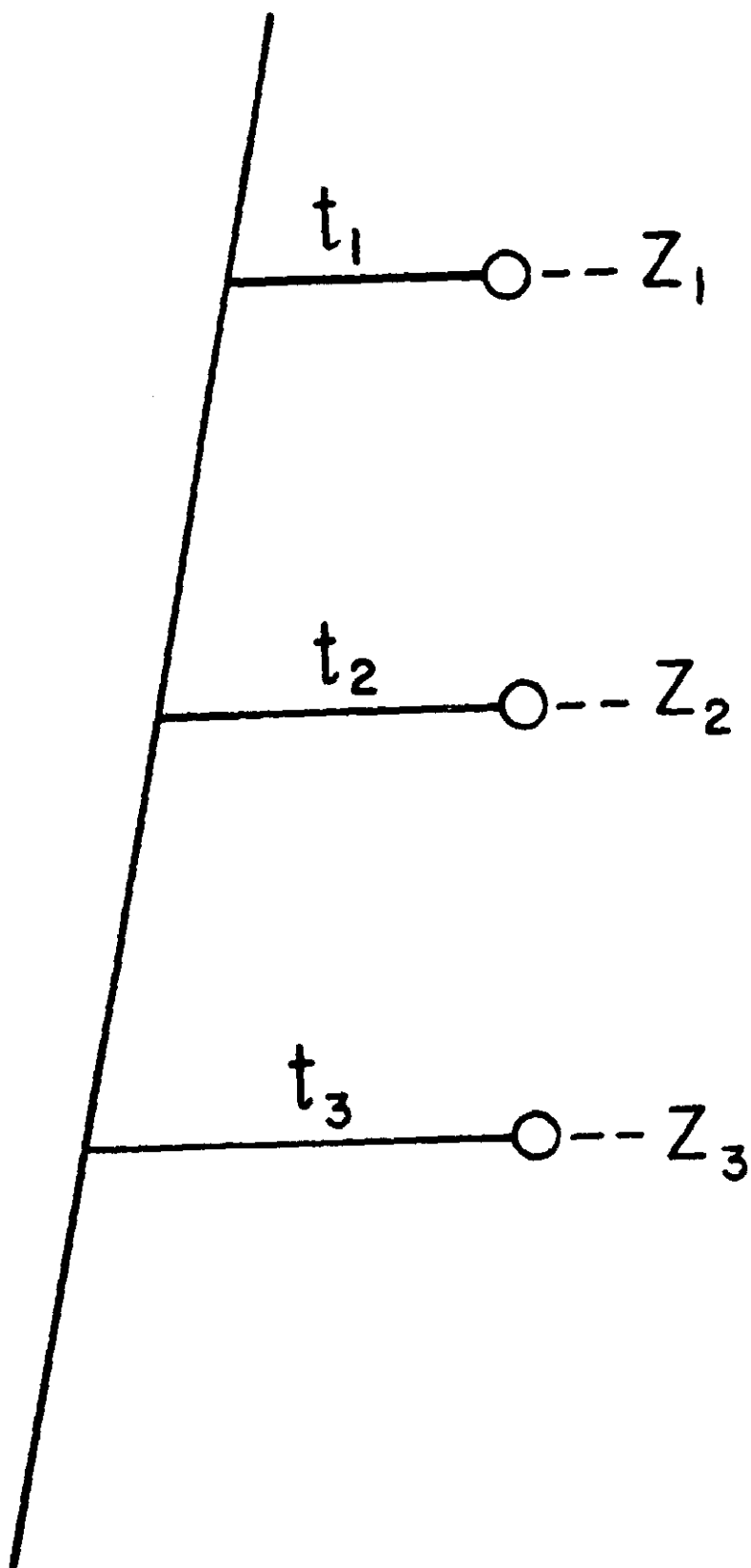


Fig. 13

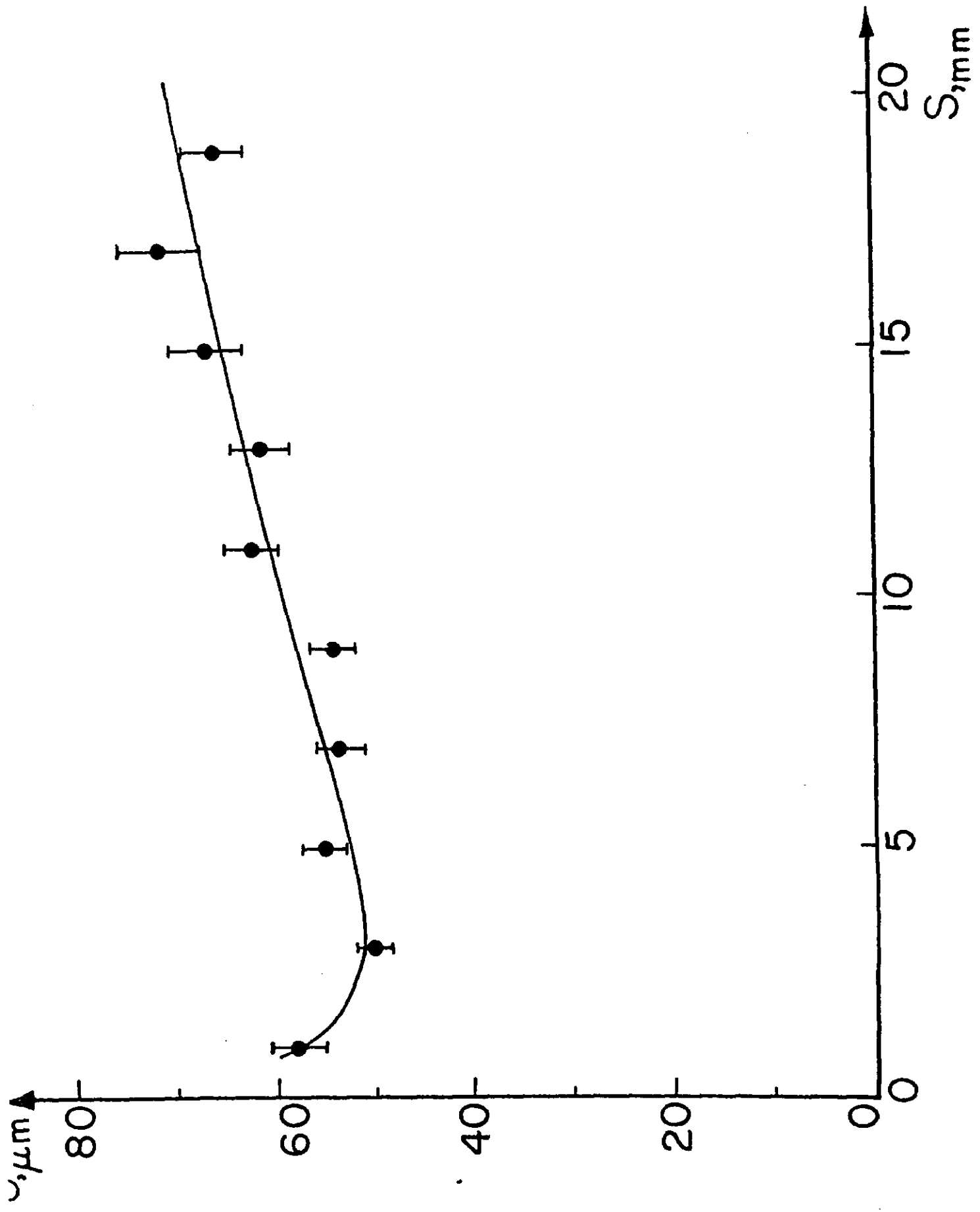


Fig 14

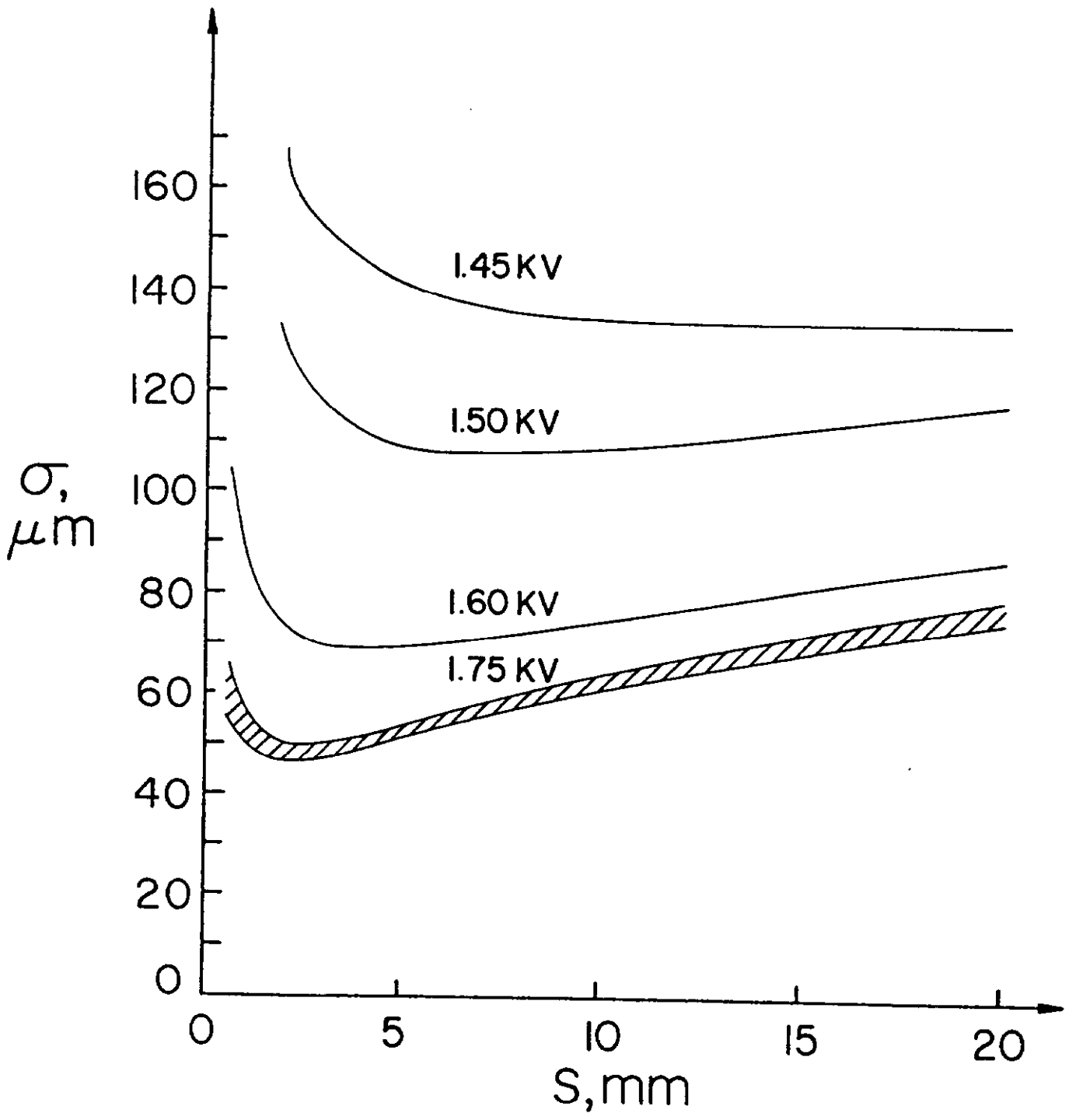


Fig. 15

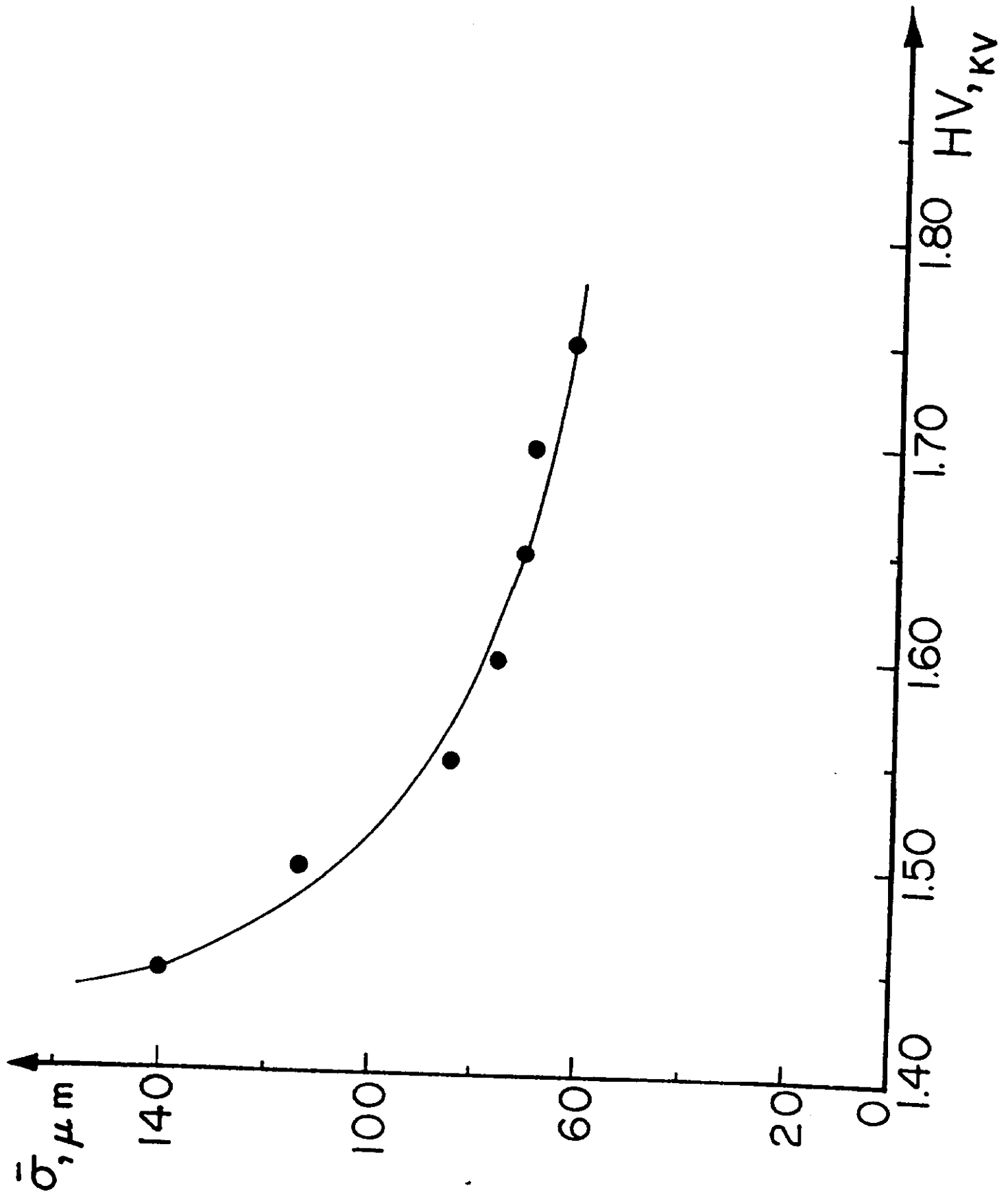


Fig. 16

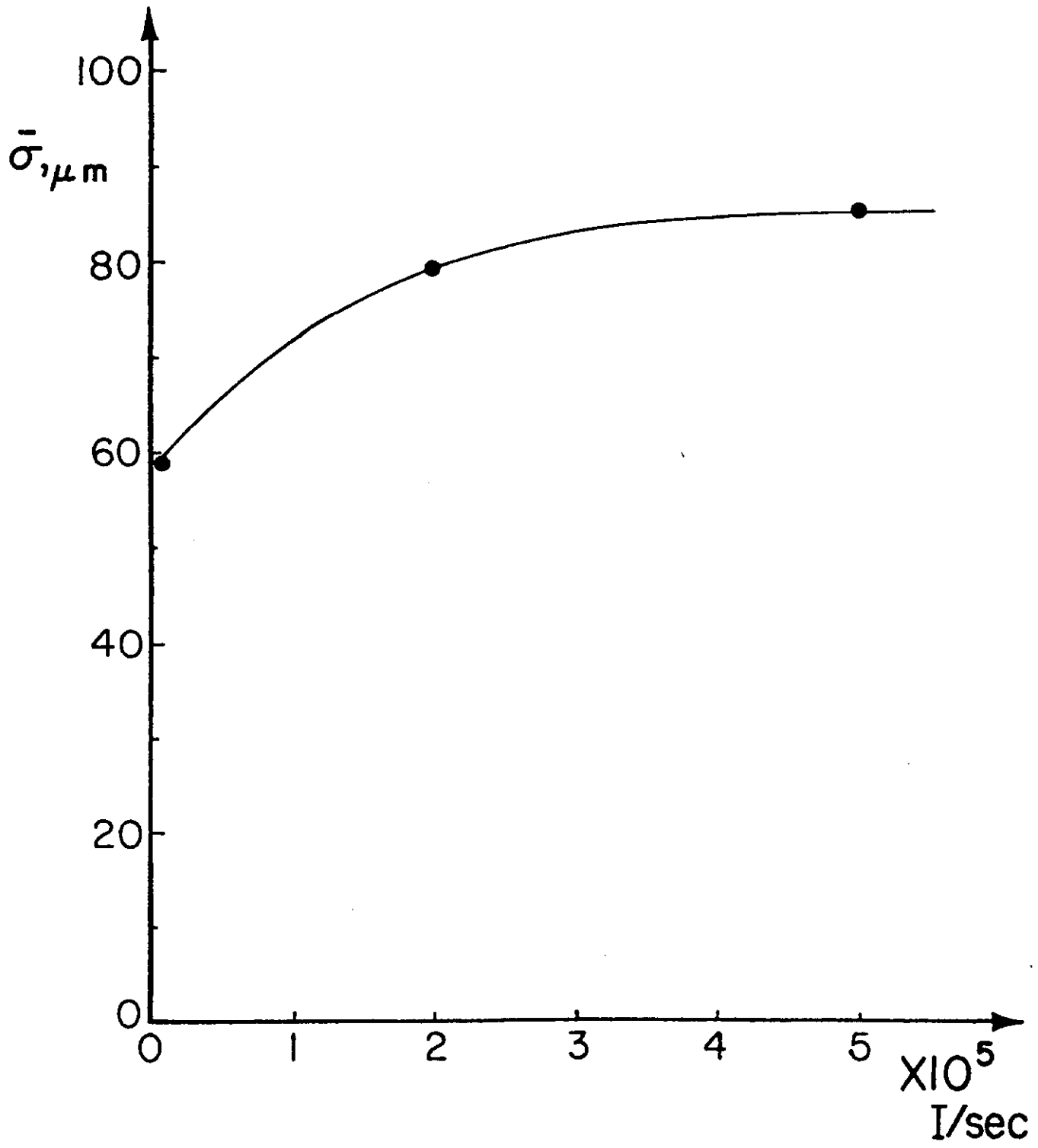


Fig. 17

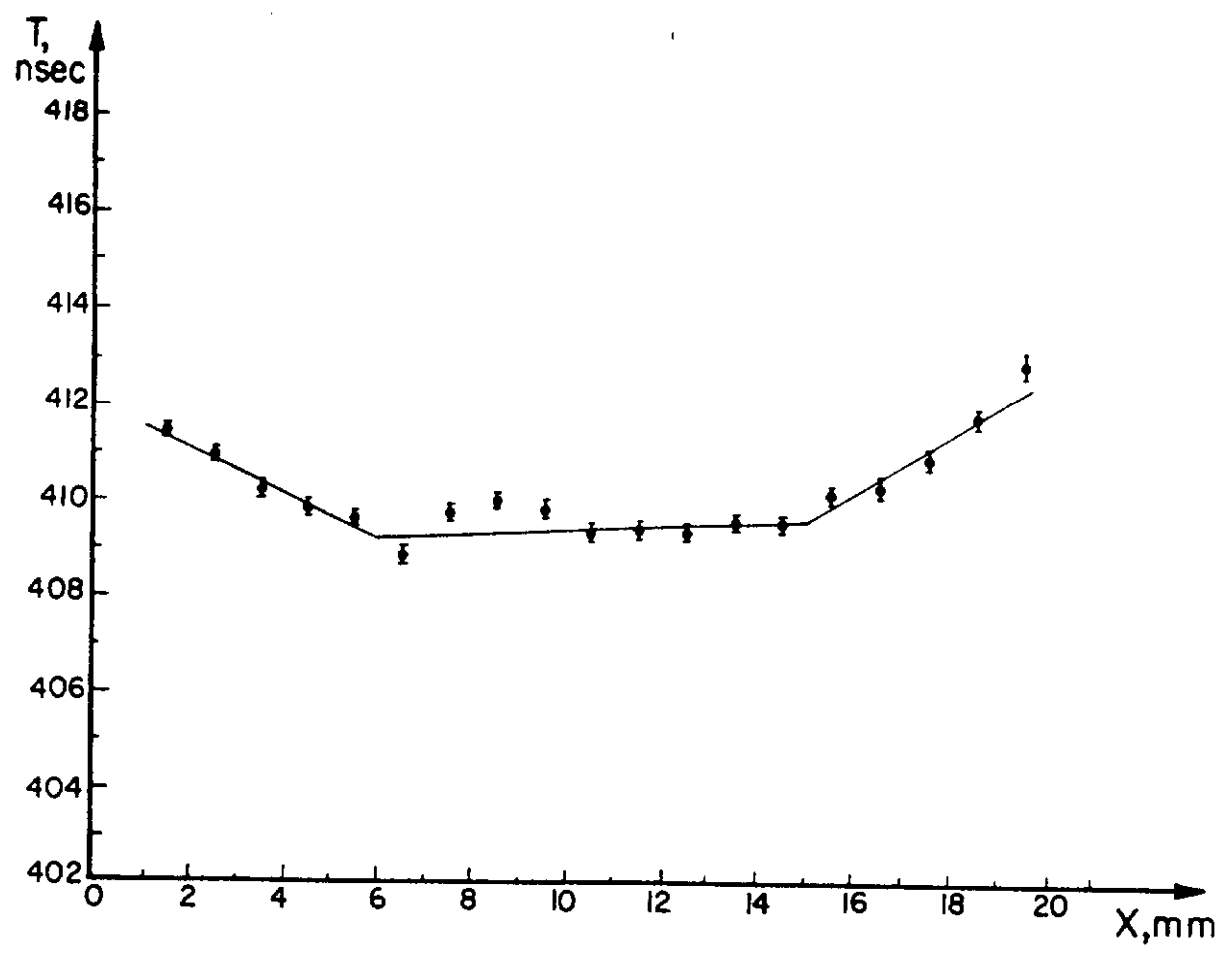


Fig. 18

